FINAL REPORT

Glass-reinforced, Recycled PET as Additive Manufacturing Feedstock

SERDP Project WP-1291

JUNE 2019

Moby Ahmed
Ambercycle, Inc.

SERDP
DOD ▪ EPA ▪ DOE

Page Intentionally Left Blank

Page Intentionally Left Blank

REPORT DOCUMENTATION PAGE

Form Approved
OMB No. 0704-0188

1. REPORT DATE *(DD-MM-YYYY)*	**2. REPORT TYPE**	**3. DATES COVERED** *(From - To)*
6/30/2019	SERDP Final Report	4/5/2018 - 4/5/2020

4. TITLE AND SUBTITLE
Glass-reinforced, Recycled PET as Additive Manufacturing Feedstock

5a. CONTRACT NUMBER
18-C-0015

5b. GRANT NUMBER

5c. PROGRAM ELEMENT NUMBER

6. AUTHOR(S)
Moby Ahmed

5d. PROJECT NUMBER
WP-1291

5e. TASK NUMBER

5f. WORK UNIT NUMBER

7. PERFORMING ORGANIZATION NAME(S) AND ADDRESS(ES)
Ambercycle, Inc.
245 W 2nd Street, Suite 11
Mesa, AZ 85201

8. PERFORMING ORGANIZATION REPORT NUMBER
WP-1291

9. SPONSORING/MONITORING AGENCY NAME(S) AND ADDRESS(ES)
Strategic Environmental Research and Development Program
4800 Mark Center Drive, Suite 17D03
Alexandria, VA 22350-3605

10. SPONSOR/MONITOR'S ACRONYM(S)
SERDP

11. SPONSOR/MONITOR'S REPORT NUMBER(S)
WP-1291

12. DISTRIBUTION/AVAILABILITY STATEMENT
DISTRIBUTION STATEMENT A. Approved for public release: distribution unlimited.

13. SUPPLEMENTARY NOTES

14. ABSTRACT
Poly (ethylene terephthalate) (PET) is a commodity thermoplastic that is predominately used in drink bottles, production of which is forecasted to reach 583.3 billion in 2021. Waste PET plastic bottles also accumulate rapidly on Forward Operating Bases (FOBs), and are currently disposed of by burning, which compromises the respiratory health of U.S. soldiers and residents of locales adjacent to FOBs. Fortunately, recycled PET (rPET) as well as its glass fiber (GF) reinforced composites have potential application as a cheap, local feedstock for fused filament fabrication (FFF) additive manufacturing (AM), which could be used to fabricate repair parts on an FOB and thus reduce time required to obtain parts.
The objectives of this study are (i) to explore the use of PET as a feedstock for FFF and (ii) to explore the effects of glass-fiber (GF) reinforcement on PET processability and final printed part properties.

15. SUBJECT TERMS
Additive manufacturing, fused filament fabrication, glass fiber, composite, recycled poly (ethylene terephthalate)

16. SECURITY CLASSIFICATION OF:			**17. LIMITATION OF ABSTRACT**	**18. NUMBER OF PAGES**	**19a. NAME OF RESPONSIBLE PERSON**
a. REPORT	**b. ABSTRACT**	**c. THIS PAGE**			Moby Ahmed
UNCLASS	UNCLASS	UNCLASS	UNCLASS	34	**19b. TELEPHONE NUMBER** *(Include area code)* 916-627-9838

Page Intentionally Left Blank

Table of Contents

Abstract 3
Introduction and Objectives 3
Technical Approach 3
Results 3
Benefits 3
1. OBJECTIVE 4
2. BACKGROUND 4
3. MATERIALS AND METHODS 4
3.1 List of Equipment 5
3.2 Filament fabrication 5
3.3 Rheology testing 5
3.4 3D printing with GF reinforced filament 5
3.5 Fiber length distribution 5
3.6 Mechanical testing 5
3.7 SEM 6
3.8 Differential scanning calorimetry (DSC) 6
4. RESULT AND DISCUSSION 6
4.1 Rheology testing 6
4.2 3D printing with rPET/GF composite filament 9
4.3 GF length distribution 11
4.4 Mechanical testing 14
4.5 Crystallinity of printed parts 18
5. CONCLUSIONS AND IMPLICATIONS FOR FUTURE RESEARCH 20
LITERATURE CITED 23

List of tables

Table 1 Printing parameters for ASTM D1708 5
Table 2 Power law index calculated for each composition 8

List of Figures

Figure 1 Shear viscosity of each rPET/GF composition 7
Figure 2 Stress vs. shear rate for rPET/GF composites 8

Figure 3 Cryofractured surface of rPET/GF filaments with varying GF loading 9
Figure 4 ASTM D1708 tensile bars printed with the custom-made deltabot printer 9
Figure 5 Cryofractured surface of tensile bars with different GF loadings 10
Figure 6 Typical triangular voids inside the printed tensile bars 10
Figure 7 Various complex parts of autonomous aerial vehicles printed with rPET/GF filaments 11
Figure 8 GF length distribution of filament and printed parts 13
Figure 9 Modulus vs. GF content 14
Figure 10 Ultimate tensile strength vs. GF content 15
Figure 11 Single layer cylinder and punched tensile bars with different orientations 16
Figure 12 Modulus vs GF content for punched tensile bars 17
Figure 13 Ultimate tensile strengths vs GF content for punched tensile bars 17
Figure 14 GF orientation at the boundary of each layer 18
Figure 15 Crystallinity measured by DSC for each composition 19
Figure 16 100 % infilled cone geometries printed with rPET/GF filaments 20
Figure 17 rPET Printed Parts Used in EcoSoar Drone Vehicle 21

List of Acronyms

PET	Poly (ethylene terephthalate)
rPET	Recycled PET
FOBs	Forward Operating Bases
FFF	Fused filament fabrication
AM	Additive manufacturing
GF	Glass fiber
DSC	Differential scanning calorimetry
K%	crystallinity

Keywords

Additive manufacturing, fused filament fabrication, glass fiber, composite, recycled poly (ethylene terephthalate)

Acknowledgements

The authors would like to thank Ambercycle Inc. for sponsoring this project, and UNIFI Inc. for providing the recycled PET flakes

Abstract

Introduction and Objectives

Poly (ethylene terephthalate) (PET) is a commodity thermoplastic that is predominately used in drink bottles, production of which is forecasted to reach 583.3 billion in 2021. Waste PET plastic bottles also accumulate rapidly on Forward Operating Bases (FOBs), and are currently disposed of by burning, which compromises the respiratory health of U.S. soldiers and residents of locales adjacent to FOBs. Fortunately, recycled PET (rPET) as well as its glass fiber (GF) reinforced composites have potential application as a cheap, local feedstock for fused filament fabrication (FFF) additive manufacturing (AM), which could be used to fabricate repair parts on an FOB and thus reduce time required to obtain parts.

The objectives of this study are (i) to explore the use of PET as a feedstock for FFF and (ii) to explore the effects of glass-fiber (GF) reinforcement on PET processability and final printed part properties.

Technical Approach

A streamline recycled PET bottle flakes were first compounded with different amount of short GF using twin-screw mixing followed by pelletizing, then filaments with different loadings of GF were extruded with Filabot EX2 filament extruder. Rheological measurements were conducted to understand the influence of GF on the composite's rheological behavior. A custom-made FFF 3D printer was used to print filaments produced from recycled PET (rPET) and GF at varying concentrations, and quality of printed parts were confirmed by scanning electron microscopy (SEM). The GF inside printed samples was recovered with TGA burn off and length distribution was analyzed by optical microscopy. Mechanical test was used to examine the performance of reinforcement, and finally differential scanning calorimetry (DSC) was used to calculate the crystallinity of printed parts.

Results

It was found that 20 wt.% of short GF tripled the viscosity of rPET as well as enhanced the shear thinning effect, and printed tensile bars showed a decreasing trend in crystallinity with glass fiber loading. It is shown that GF leads to an increase in both modulus and tensile strength of the printed parts. However, compared with the modulus increase (71 %), the increase in tensile strength is relatively small (25%), mainly due to the significant fiber break down as shown by the glass fiber length distribution. Qualitative evaluation of the printability of this recycled PET as well as its glass fiber reinforced composite is demonstrated by printing several complex geometries, including components for an autonomous air vehicle (drone).

Benefits

These results suggest a promising future for this technique to be applied in resource-poor areas or forward operating base (FOB) as a method to turn waste water bottles directly into printed functional parts, which could greatly shorten the wait time for repair parts delivery and reduce raw material demand on site.

1. OBJECTIVE

The overall goal of this research was to explore the use of recycled PET (rPET) as a fused filament fabrication (FFF) feedstock. In addition to experimenting with printing neat rPET, the team also plan to incorporate rPET with glass fiber (GF) to explore its effects on printability and the mechanical properties of the resulting products. Specifically, to evaluate the influence of GF on rheology, crystallinity and reinforcement effects. Products featuring complex geometries will be printed with rPET and its GF composites; in order to demonstrate great potential for this material to be 3D printed via FFF.

2. BACKGROUND

The global production rate of plastic bottles is around one million per minute, and the number is estimated to jump another 20% by the year 2021 [1]. Further, more than 70 % of poly(ethylene terephthalate) (PET) bottles produced are not recycled [2]. As a high performance and well-developed plastic, the growing market demand for PET and its corresponding products seems to have an irreconcilable conflict against sustainability. On forward operating bases (FOBs), waste PET bottles accumulates at a rate of 0.367 kg/day·soldier, and represent 5.1% of the total waste generated [3]. Currently the waste stream is disposed simply by burning, which compromises the health of the local environment and soldier. One pathway for reusing waste PET could be as a feedstock for additive manufacturing (AM, also referred to as 3D Printing). Directly 3D printing from waste PET on FOBs could both reduce harmful waste and also reduce the logistics tail by negating the need for raw materials for on-site AM and reducing the need for resupply of spare parts and shipment of new parts for emerging solutions.

Fused Filament Fabrication, a modality of AM that produces parts by selectively hot-melt extruding thermoplastic filament in a layer-wise fashion, is a candidate technology for processing recycled PET. FFF systems are cost-effective [4, 5], simple in machine configuration, and feature a breadth of build envelopes – ranging from industrial-scale (~20x20x20 in.) to desktop-scale (4x4x5 in.). FFF is therefore easily deployable to resource-poor areas that require onsite manufacturing and is capable of making robust products of sufficient quality for end-use application.

However, to successfully transform FFF from a “rapid prototyping” technology into a “manufacturing” technology requires exploration of new printable materials [6]. Currently, the most popular materials for FFF are amorphous thermoplastics like ABS and PLA [7]. FFF printing with semi-crystalline materials like PP [8, 9] or HDPE [10, 11] have been reported, but the results were unsatisfactory. Generally, semi-crystalline materials have a large shrinkage ratio due to the significant change in specific volume when they crystallize, which leads to unacceptable warpage during printing. However, unlike the unprintable HDPE or PP, PET has a relatively smaller change in specific volume [12-14], and also a much slower crystallization rate [15], which leads to a smaller shrinkage during printing. And with its high recyclability [15, 16] and good melt flowability, these properties make rPET a promising candidate for FFF.

3. MATERIALS AND METHODS

3.1 List of Equipment

The equipment Virginia Tech used are as listed:

Major equipment: vacuum dryer, plastic granulator, twin screw extruder, pelletizer, filament extruder, filament 3D printer

Ancillary requirements: power, water, glass fiber (needs to be shipped to FOBs)

3.2 Filament fabrication

The raw materials used to create the FFF filaments are recycled PET (rPET) flakes (provided by UNIFI) and Owens Corning 183F short glass fiber (GF). In order to promote uniform mixing with glass fiber, the rPET flakes are first granulated to a smaller size. Both ground rPET flakes and short GF were dried overnight at 90° C under vacuum, then mixed by shaking before extruded with a Leistritz ZSE 18 twin screw extruder with a water bath. The extruder's eight temperature-controlled zones were set as 220° C, 230° C, 230° C, 240° C, 240° C, 240° C, 250° C, 250° C from feed port to die, and screw speed was set to 100 rpm. The extrudate was pelletized and vacuum dried at 120° C overnight. A Filabot EX2 filament extruder was used together with a custom-made conveyer belt for making rPET/GF filament. The extruder's temperature was set to 270° C, and both 1.75 mm or 2.85 mm filament were processed to match differing printer's configurations.

3.3 Rheology testing

Evaluations of rPET/GF pellets' rheology were conducted with a TA instrument HR1 Discovery Hybrid rheometer at 270° C using 25 mm parallel plates at a 1 mm gap. Flow sweep was selected as experiment procedure with a shear rate ramping from 1 to 100 s^{-1}.

3.4 3D printing with GF reinforced filament

ASTM D1708 tensile bars were printed on blue tape with a custom-made, delta-bot FFF 3D printer. The Slic3r software was used together with Repetier-Host. A 0.6 mm E3D hardened steel nozzle was installed to prevent nozzle damage from GF abrasion. The printing parameters are listed in Table 1. In addition to the tensile bars for mechanical testing, several other geometries were also printed to demonstrate the printability of this material.

Table 1 Printing parameters for ASTM D1708

Nozzle temperature (° C)	*Bed temperature (° C)*	*Shell perimeters*	*Infill density*	*Fill pattern*	*Speed (mm/s)*	*Fan cooling*
270	Room temperature	3	100%	Rectilinear	15	N/A

3.5 Fiber length distribution

GF was recovered from both filament and printed parts using TGA (TA Q50) at 600° C for 4 hours, then dispersed in a small amount of distilled water for better observation. Images from the optical microscope (ZEISS Axio Vert.A1 Inverted Microscope) were processed with the software ImageJ to analyze the length distribution of recovered GF.

3.6 Mechanical testing

Uniaxial tensile testing for the printed ASTM D1708 tensile bars were conducted with an Instron 5984 Universal Testing System at a displacement rate of 1mm/min, for each composition

seven tensile bars were tested to obtain the average value. To determine the level of anisotropy in the mechanical properties of printed specimens, a smaller Instron machine (Instron 5500R) was used due to the smaller size (10 mm gauge length and 3 mm width) of the punched single layer tensile bar.

3.7 SEM

In order to examine the GF dispersity and the quality of printed parts, both rPET/GF filaments and printed tensile bars were cryofractured with liquid nitrogen, then sputter coated with Cressington 208HR sputter before probed using a LEO (Zeiss) 1550 field-emission SEM.

3.8 Differential scanning calorimetry (DSC)

The crystallinity of printed ASTM D1708 tensile bars was measured using a differential scanning calorimetry (TA Q20). Specimens were taken from the same position of each tensile bar and tested with a heating rate of 10° C/min. Crystallinity (K%) was calculated through the following equation:

$$K\% = \frac{\Delta H_m - \Delta H_{cc}}{\Delta H_f \times V_{rPET}}$$

where ΔH_m and ΔH_{cc} is the area of the melting peak and cold crystallization peak, respectively. V_{rPET} is the volume fraction of the rPET in the composite. ΔH_f is the heat of fusion for 100% crystallized PET, in this study, a ΔH_f value of 120 J/g is used [17].

4. RESULT AND DISCUSSION

4.1 Rheology testing

The shear viscosity of rPET/GF compositions at varying GF wt% was measured at steady state, as shown in Fig. 1

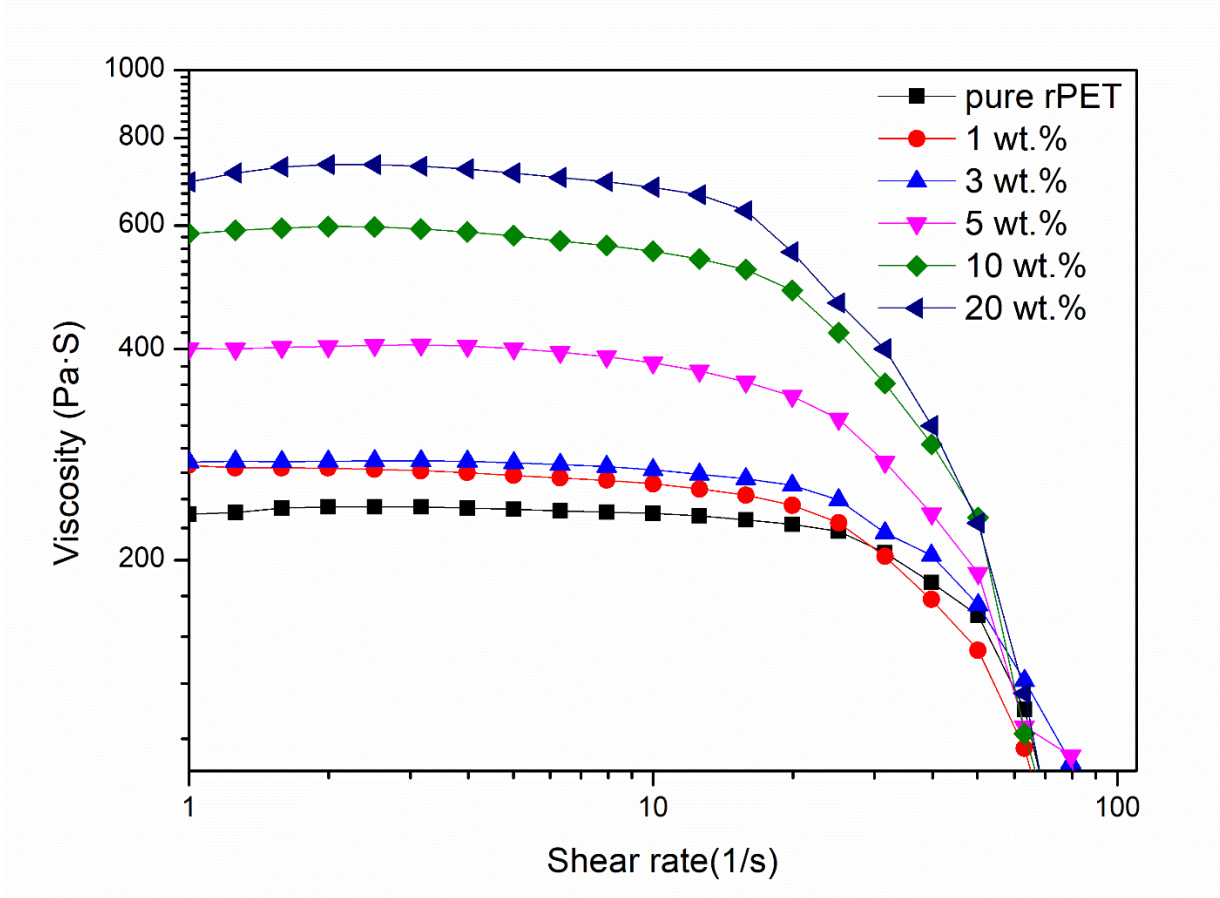

Figure 1 Shear viscosity of each rPET/GF composition

For the low shear rate region (1 to 10 s^{-1}), all the samples were showing a Newtonian fluid behavior, as the shear viscosity remained almost constant versus the shear rate. Such a Newtonian behavior would suggest that the GF filler was well incorporated in the polymer matrix [18]. Adding fillers to the polymer matrix can effectively increase the material's viscosity [18-20]. As seen in Fig. 1, the zero-shear viscosity for pure rPET is around 250 Pa·s, relatively lower to virgin PET (~700 Pa·s; [21, 22]). As the loading of GF increases, the viscosity also increases; at 20 wt.% GF the viscosity nearly tripled to around 720 Pa·s. Higher viscosity can increase resistance to bead deformation and improvement of bridging performance during printing [23].

As the shear rate increases, all specimens start to show a shear-thinning characteristic, which can be observed in the stress vs. shear rate diagram shown in Fig. 2.

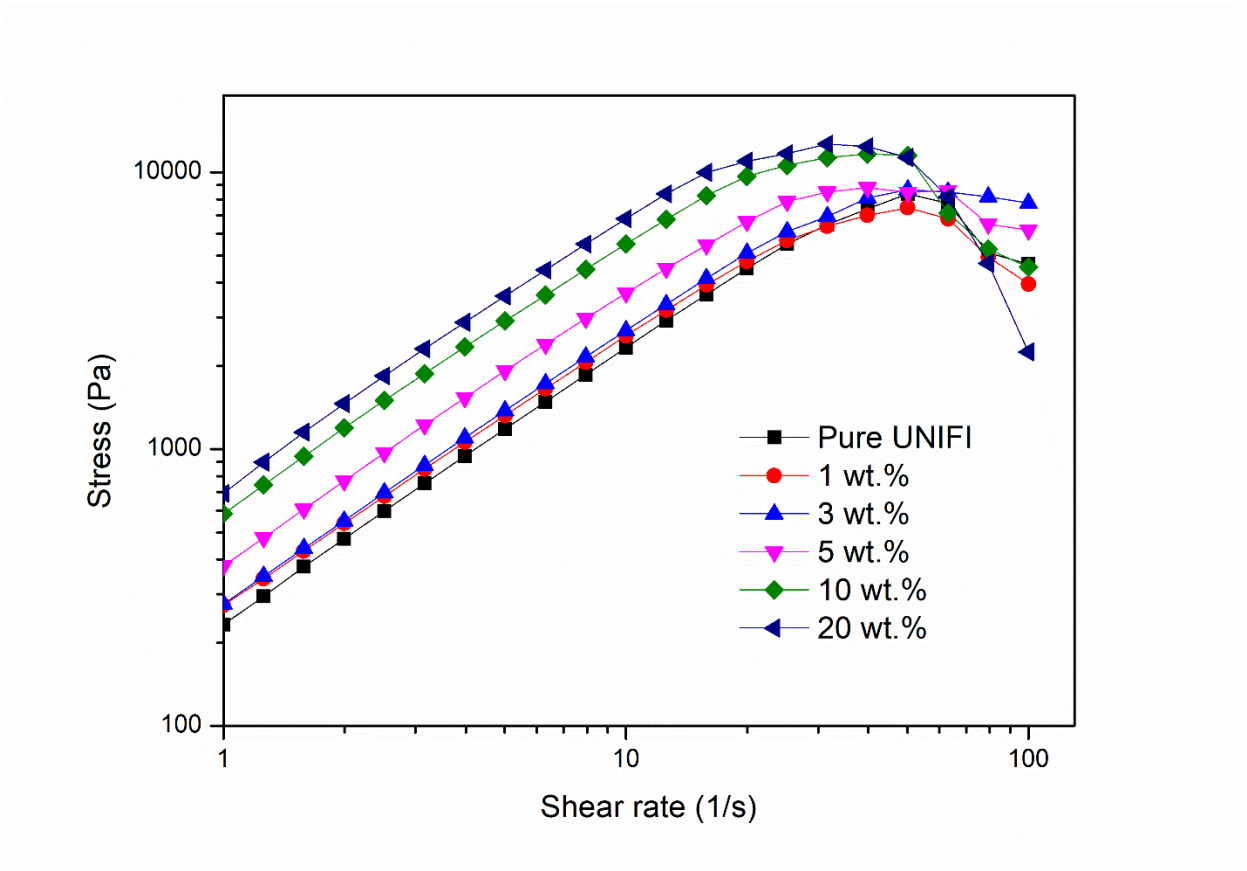

Figure 2 Stress vs. shear rate for rPET/GF composites

At a shear rate above 20 s^{-1}, the slope of the stress curve for all samples start to decrease, indicating a typical shear thinning behavior. Note that if the shear rate further increases above 50 s^{-1}, the samples will start to have gap failure (indicated by the decreasing of stress), so only data points between 20 s^{-1} and 50 s^{-1} are used to fit into the power law model. The power law index was calculated using the Oswald de Waele Power Law model where $\tau = K\gamma^n$. K = viscosity constant, τ = shear stress, γ = shear rate, and *n* = power law index. The fitted results are listed in Table 2.

Table 2 Power law index calculated for each composition

Composition	Power law index, *n*
Pure UNIFI rPET	0.588582
1 wt.% GF	0.454037
3 wt.% GF	0.505619
5 wt.% GF	0.262884
10 wt.% GF	0.183609
20 wt.% GF	0.122191

Generally, as the content of GF increases, the power law index decreased, which corresponds to GF enhancing the shear-thinning behavior of the material. Such results are not counterintuitive since GF will significantly increase the viscosity of the composite material; however, when under

the influence of shear flow, GF will gradually orient along the flow direction, which decreases viscosity. Thus, the more GF content, the more significant this phenomenon will be.

4.2 3D printing with rPET/GF composite filament

1.75 mm rPET/GF filament was made with Filabot EX2 filament extruder and a custom-made conveyer belt (installed with cooling fan). Fig. 3 show the cryofractured surfaces of filaments with different GF loadings. Over the fractured surface, no bundles of GF were observed, indicating good compatibility between 183F short GF and rPET matrix. In addition, it is observed that the GF are all aligned with the direction of filament extrusion.

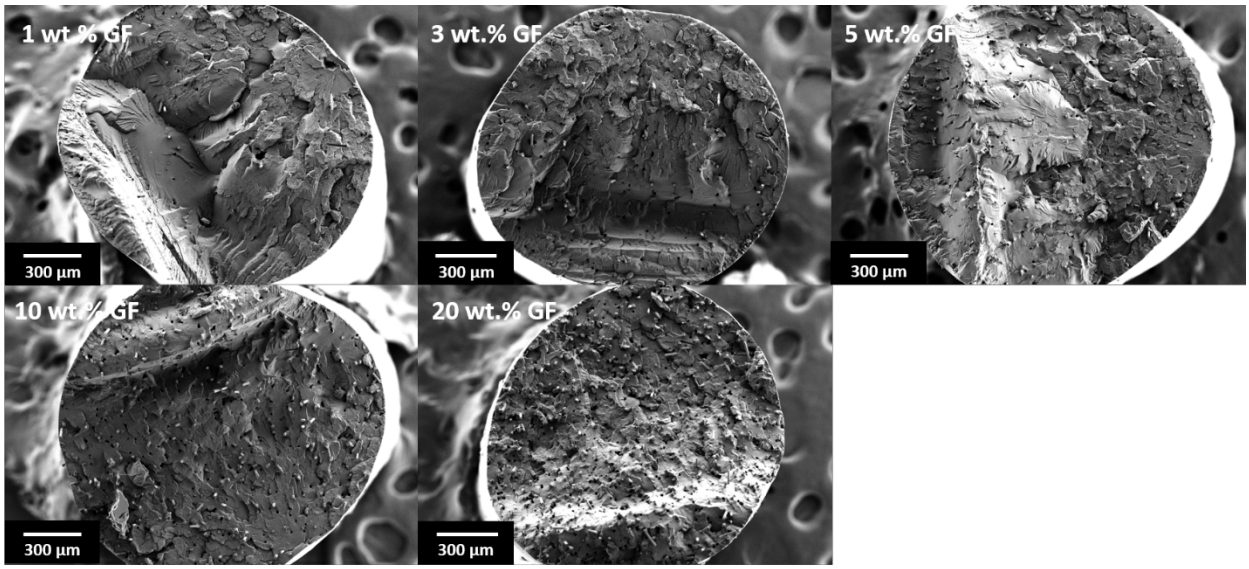

Figure 3 Cryofractured surface of rPET/GF filaments with varying GF loading

A custom-made FFF printer was used to print specimens with these composite filaments. To further examine the quality of different rPET/GF filament printed parts, printed tensile bars (Fig. 4) were cryofractured and probed under SEM (Fig. 5). Fig. 6 provides a magnified view of the fracture surfaces imaged in Fig. 5.

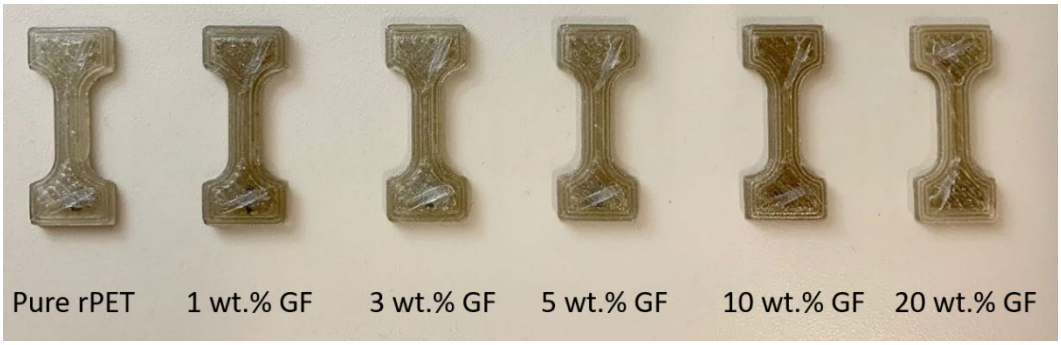

Figure 4 ASTM D1708 tensile bars printed with the custom-made deltabot printer

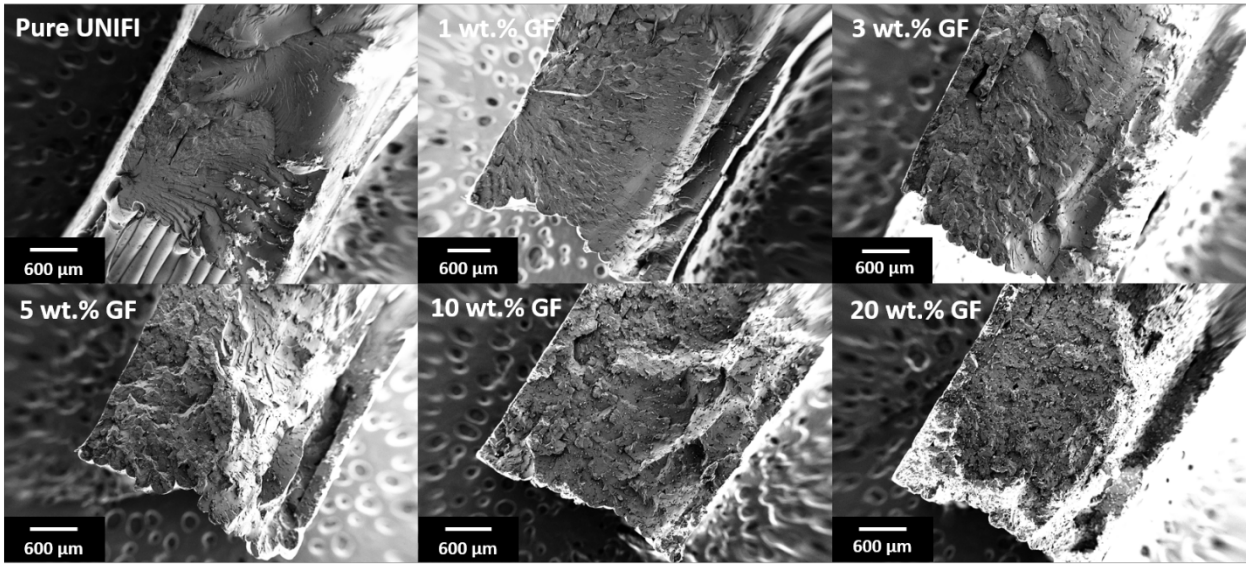

Figure 5 Cryofractured surface of tensile bars with different GF loadings

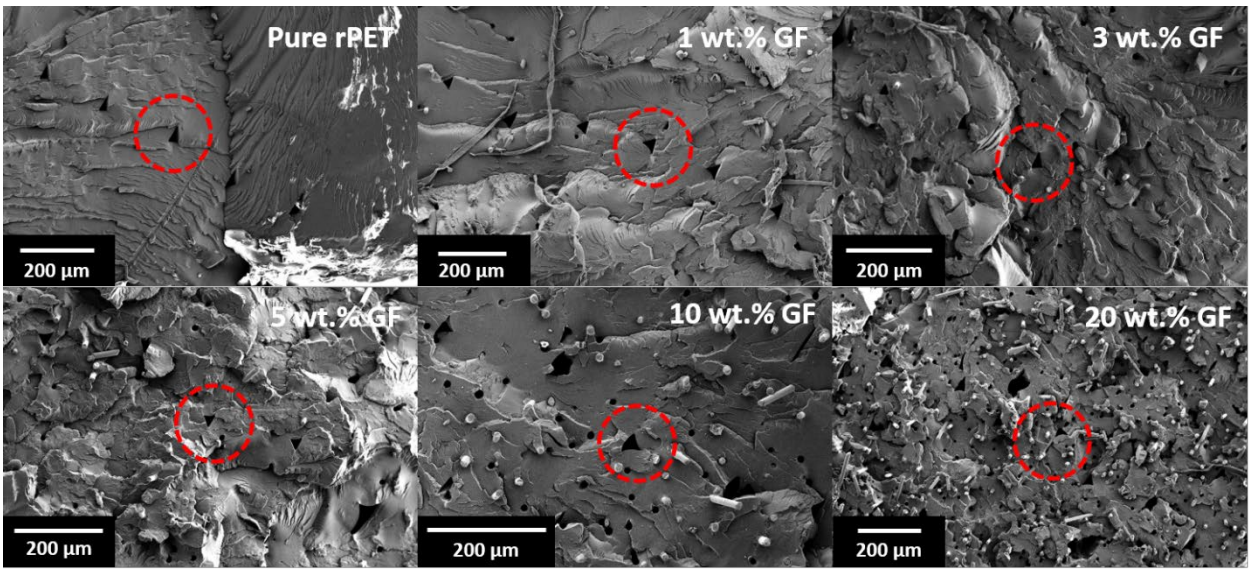

Figure 6 Typical triangular voids inside the printed tensile bars

In Fig. 6, the triangular voids typical of fused filament fabrication are highlighted by red circles; such voids originate from the insufficient contact between adjacent printed roads since the printed road has a rounded rectangle cross-sectional shape. The size of this void defect is much smaller compared with the overall dimension of the printed parts. In Fig. 5 it can be seen that all the fractured surfaces showed a typical ductile fracture characteristic. And the fractured surface is generally dense and solid, with no evident debonding between printed layers.

It is also observed that, on the fracture surface, most of the glass fibers are oriented outwards. This is because, during both the filament extrusion and the printing process, the material was forced to flow through a small orifice, during which the GF aligned with the direction of the flow

field. This gives rise to an anisotropy of reinforcement in the printed part, which is further investigated in Section 4.4.

To demonstrate the printability of this rPET/GF composite, several other geometries were printed, as shown in Fig. 7. All of the printed parts presented a surface finish and mechanical properties suitable for part production.

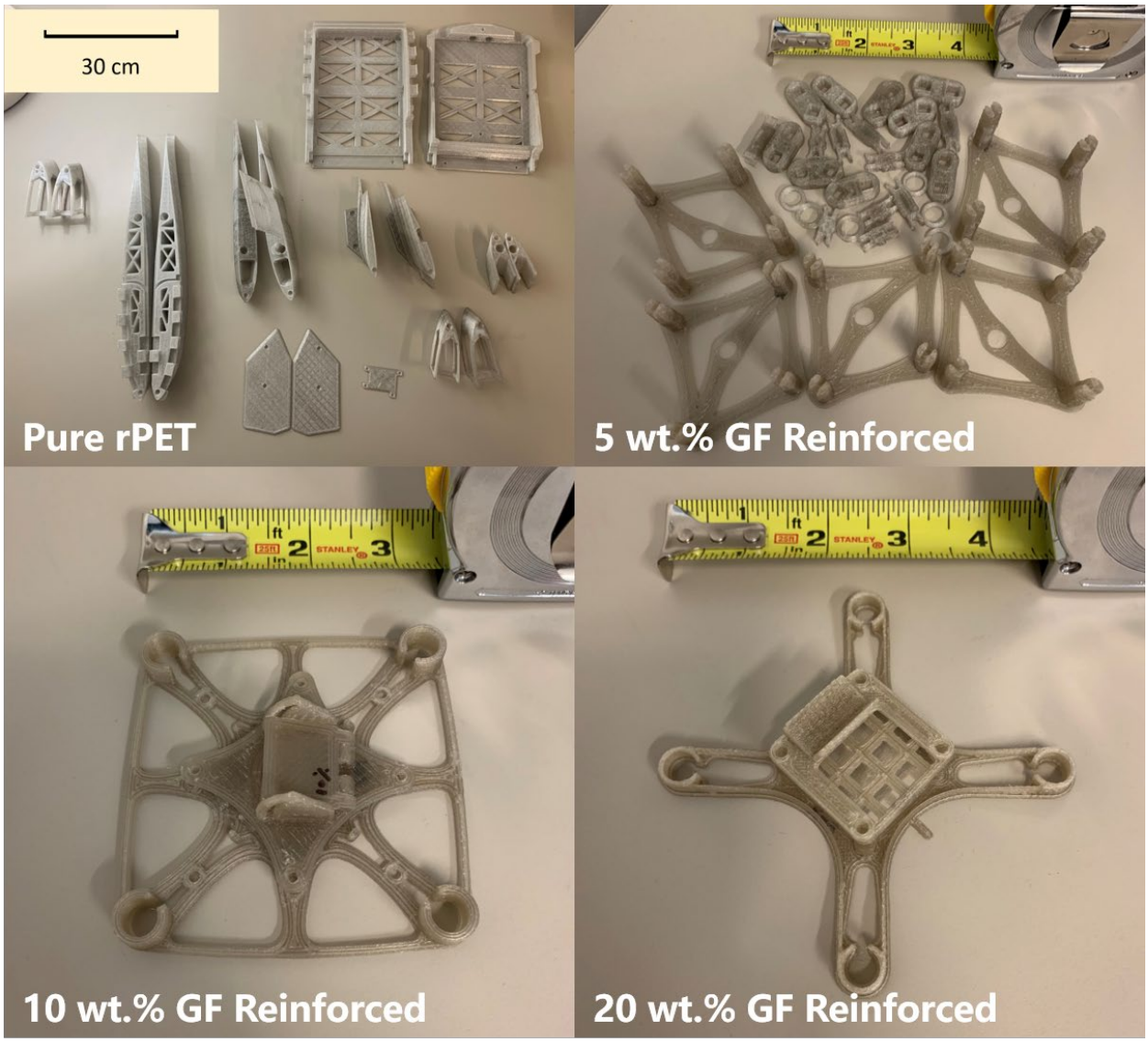

Figure 7 Various complex parts of autonomous aerial vehicles printed with rPET/GF filaments

4.3 GF length distribution

The residual length of GF is critical to its reinforcing ability. However, the GF usually breaks down during the mixing or extrusion process. TGA was used to explore the status of reinforcement GF filler by holding the composite filaments at 600° C for 4 hours, which burned off the rPET matrix and enabled recovery of the GF from both filaments and printed parts. The

recovered GF were then dispersed in distilled water for better imaging with optical microscope; length measurements were completed by an image processing software (ImageJ). Fig. 8 is a comparison between the GF length distribution of filament and printed parts.

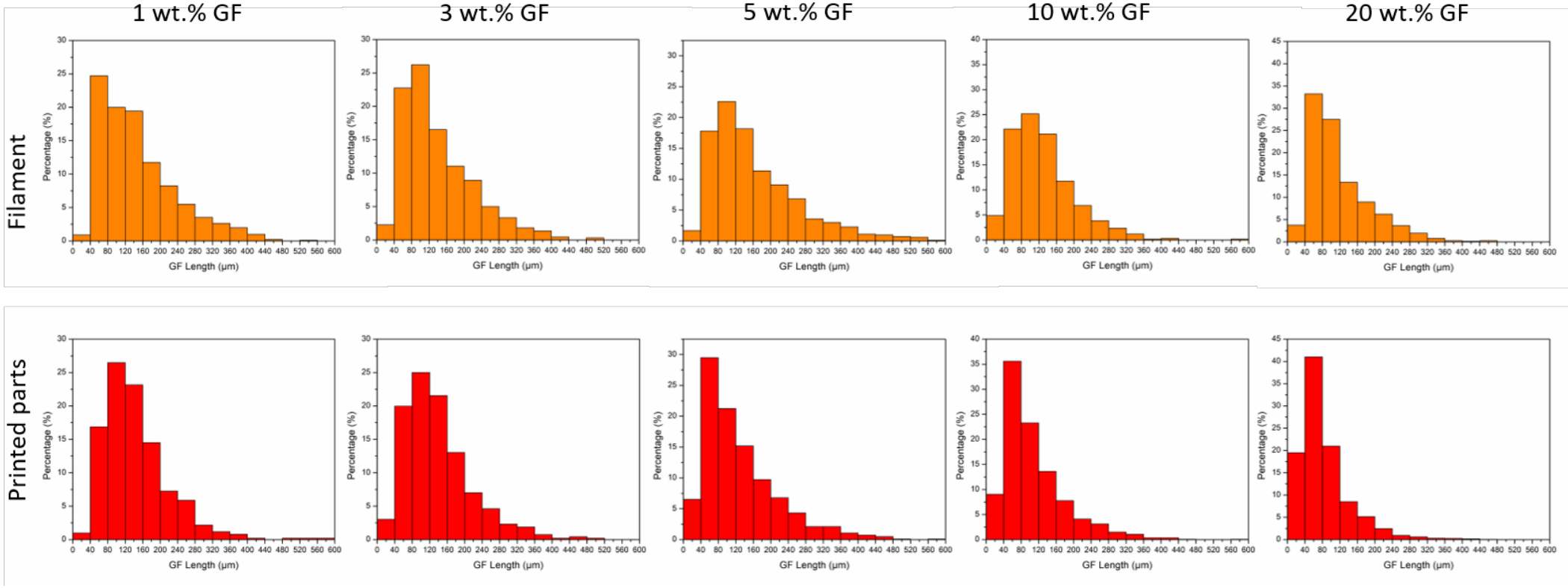

Figure 8 GF length distribution of filament and printed parts

For both filaments and printed parts, the largest portion of residual GF is all below 240 μm. This significant reduction in fiber length is due to the multiple extrusion processes: the materials were first extruded from the twin screw extruder, then extruded again with Filabot EX2 filament extruder, and for the printed parts, a third extrusion from the print head is applied to the filament. This is reflected in Fig. 8 where the printed parts featured a much smaller portion of larger fibers than those seen in the filament. This fiber length reduction is closely related to the macroscopic mechanical performance, which is explored in the following section.

4.4 Mechanical testing

The results of uniaxial tensile test of ASTM D1708 tensile bar printed with rPET/GF filaments at various GF wt% are plotted in Fig. 9 and Fig. 10.

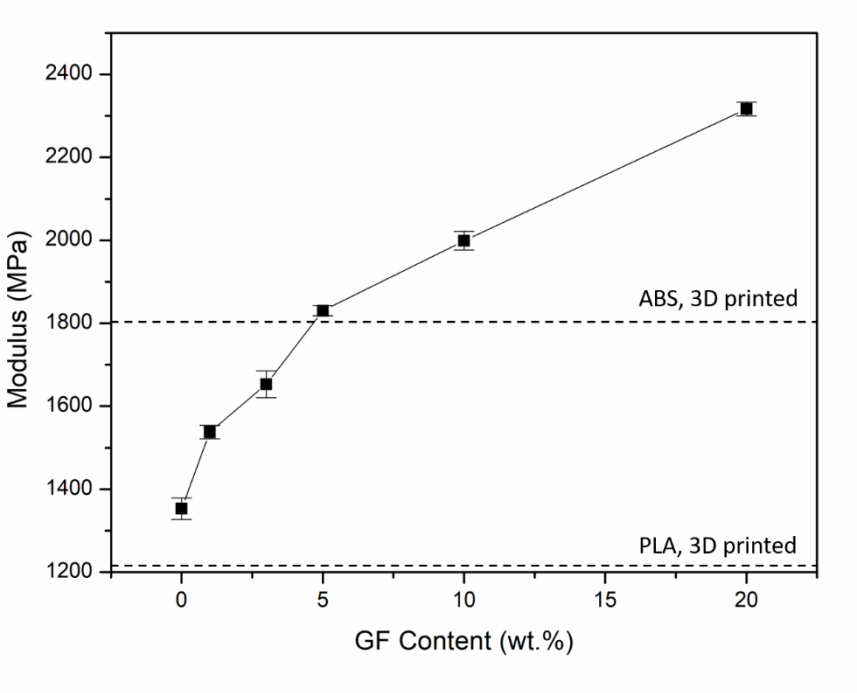

Figure 9 Modulus vs. GF content

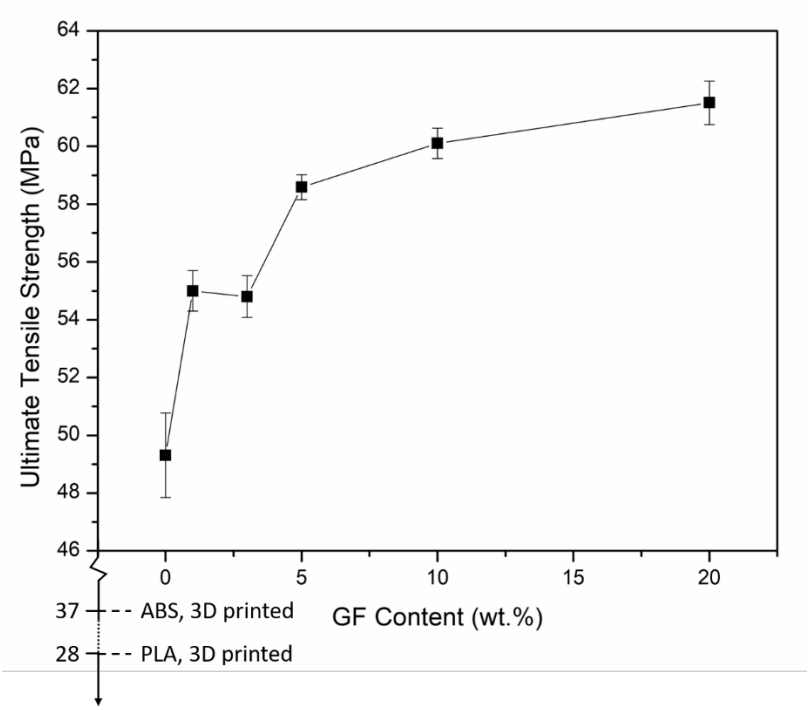

Figure 10 Ultimate tensile strength vs. GF content

It is observed that the modulus of printed rPET/GF composites increased with GF content, and with 20 wt.% GF, the modulus nearly doubled (Fig. 9). Usually, the macroscopic properties of composite material are affected by factors including interfacial adhesion, shape, and orientation of dispersed phase [24, 25]. In the SEM images of cryofractured surface (Fig. 5 & 6), the good dispersion and interfacial adhesion of GF inside printed parts were confirmed, and those well-dispersed GF increased the material's stiffness without causing a catastrophic loss in ductility (i.e., the printed tensile bars with 20 wt.% GF still showed a semi-ductile failure during the tensile test). The increase in tensile strength is limited compared with modulus (Fig. 10) due to the reduction of GF size reduction over the course of multiple extrusions.

According to the theory of Kelley and Tyson [17, 26-28], the critical fiber length l_c for reinforcement is calculated as

$$\frac{l_c}{d} = \frac{\sigma_{fu}}{2\tau_y}$$

where σ_{fu} is the ultimate fiber strength (3100 - 3800 MPa according to Owens Corning [29], here 3450 MPa is used) and τ_y is the interfacial shear strength (45 MPa for the perfectly bonded condition with PET [17]); thus l_c is calculated to be 421.6 um. According to the fiber length distribution (Fig. 8), most of the fibers inside the filament are shorter than this calculated l_c value. When fibers are shorter than the critical length, they tend to pull out under tension rather than fracture, thus the increase in ultimate tensile strength is not as significant.

The mechanical properties of printed rPET/GF tensile bars are also compared with two most popular 3D printing materials (ABS [30] and PLA [31]) in Fig. 9 and Fig. 10. It can be seen that pure rPET already provide larger modulus than PLA, and with only 5 wt.% GF, rPET/GF composite can achieve larger modulus than ABS. The ultimate tensile strength is always larger than ABS and PLA even without GF reinforcement. These results successfully demonstrated the outstanding performance of this recycled PET and its GF composites.

As mentioned earlier in this section, the orientation of the dispersed phase is another key factor that affects the composite's macroscopic property. Inside the printed parts, the GF was well-aligned with the printing direction (Fig. 6), which leads to an increase in the anisotropy of the material. To further investigate this phenomenon, several single layer heptagon cylinders was printed with rPET/GF filaments, and small tensile bars with different orientation were punched out. Fig. 11 is an example of pure rPET printed single layer cylinder and the direction for punching tensile bars.

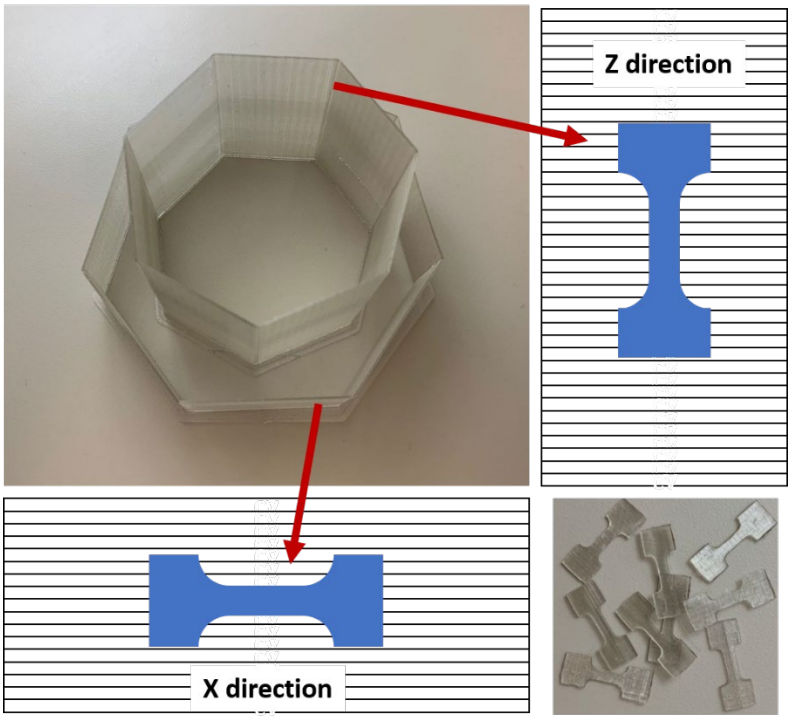

Figure 11 Single layer cylinder and punched tensile bars with different orientations

Tensile test results for these small tensile bars are shown in Figs. 12 and 13, along with the tensile data from the printed ASTM D1708 tensile bars for comparison.

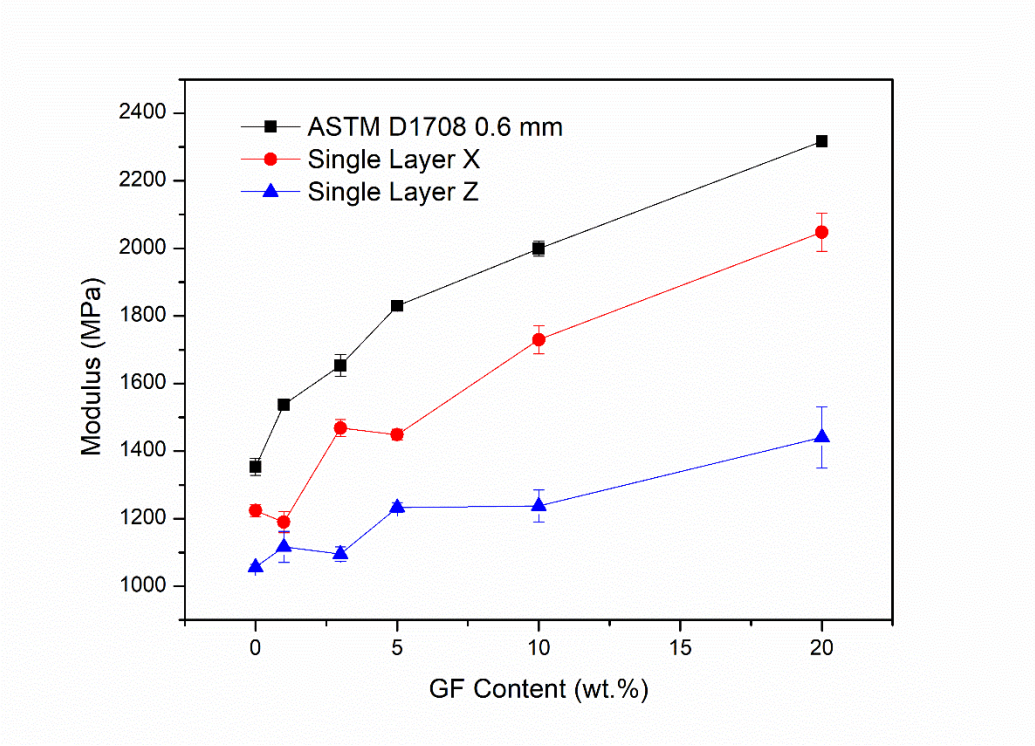

Figure 12 Modulus vs GF content for punched tensile bars

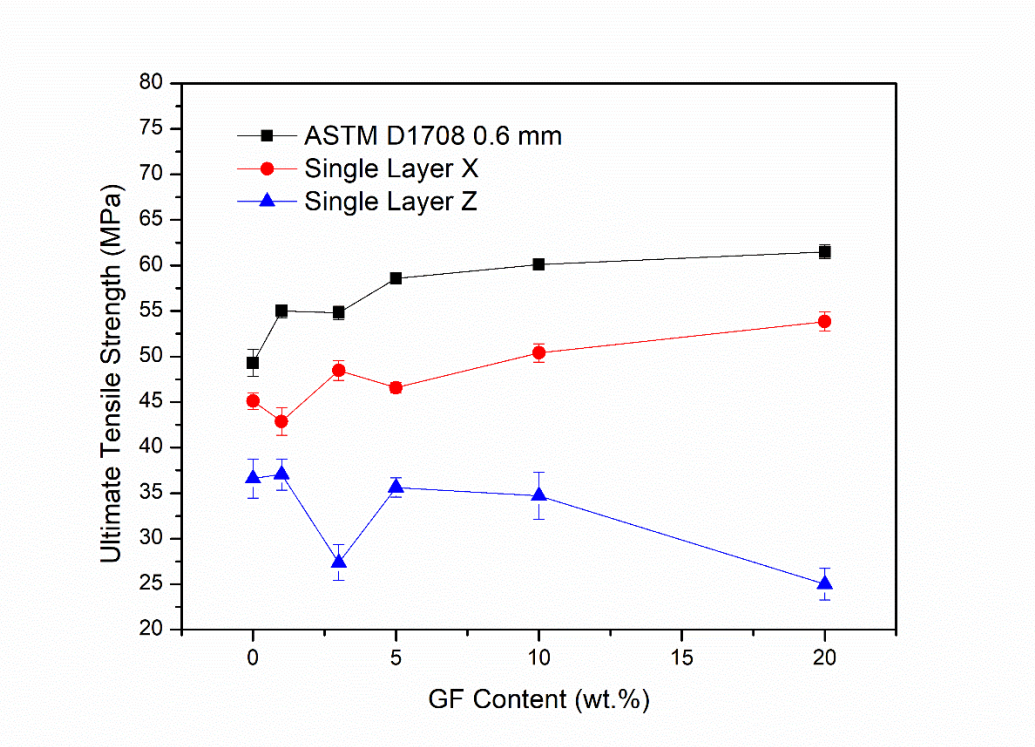

Figure 13 Ultimate tensile strengths vs GF content for punched tensile bars

As seen in Fig. 12, the modulus of X and Z specimens was similar at lower GF concentration, which indicates very good adhesion of the printed rPET layers. As GF content increased, the difference in tensile modulus between two orientations gradually increases. Given that the GF inside the printed parts is oriented along the printing direction, it is reasonable that more GF will lead to increased anisotropy in modulus.

By comparing the tensile strengths of specimens in Fig. 13, it is also found that increasing the content of GF decreases the ultimate tensile strength in the Z direction, which corresponds to a decrease in interlayer adhesion. It is shown that when GF reinforced PET exits an orifice, the variation of wall shear rate can change the orientation of GF on the surface of the extrudates [32]. Wall shear rate can be calculated by:

$$\gamma_w = \frac{4Q}{\pi R_c^3}$$

where Q is the volumetric flow rate (estimated by 15 mm/s print speed × 0.2 mm layer height × 0.6 mm extrusion width). R_c is the radius of the flow channel, taken to be the radius of the nozzle (0.6 mm). Finally, the calculated wall shear rate is 85 s^{-1}, under which condition, according to the literature [32], the GF will still orient parallel to the flow direction, rather than protrude out of the surface of the extrudates, as illustrated in Fig. 14.

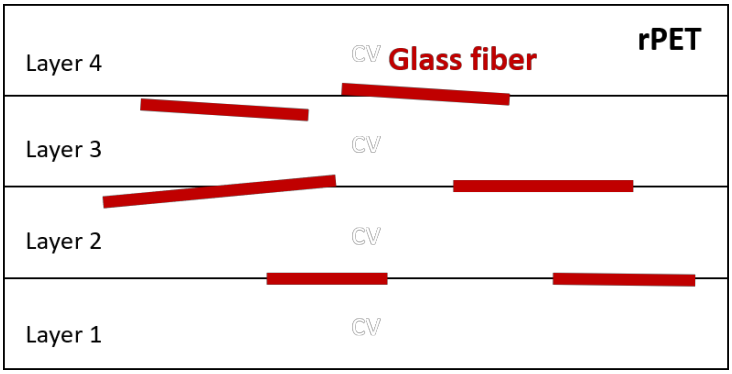

Figure 14 GF orientation at the boundary of each layer

In this situation, the addition of GF decreases the contact area of rPET matrix between printed layers, which leads to a decrease in the interlayer bonding strength and results in the decrease of the ultimate tensile strength along the Z direction.

4.5 Crystallinity of printed parts

Currently, almost all of the off-the-shelf PET FFF filaments are PET-G filament, which is molecularly modified to be amorphous. While PET itself is a semi-crystalline polymer, so is its recycled version: rPET. The crystallinity of semi-crystalline polymers has a large effect on its mechanical behavior. A low crystallinity PET or rPET is flexible and ductile, while higher crystallinity leads to brittle fracture under impact. To understand the influence of adding GF on crystallinity, DSC measurements were conducted on the printed ASTM D1708 tensile bars. The specimens for DSC were taken from the same position on each tensile bar to make sure their data are comparable.

Fig. 15 is the measured crystallinity plotted versus the GF content. An overall decreasing trend is seen here, but the crystallinity data scattered over a wide range. Literature has very contradictory findings on how GF affects the crystallinity of the PET/GF composites. Some report that the crystallinity of PET will decrease after incorporation of GF [19, 33, 34], others found that increasing the content of GF actually increased the degree of PET's crystallinity [20]. It seems more authors have found that GF will decrease the crystallinity of PET, which is in accordance with what is observed in this study. It is worth noting that, Veronika and Ludwig reported that adding GF to PET will cause a decrease in crystallinity under isothermal crystallization condition [34], but when GF is added to PET matrix with additives like plasticizers or nucleating agents, the final crystallinity under isothermal crystallization will not be affected by the GF [35]. For rPET used in this study, it is very likely some of the recycled flakes will contain additives, thus although a decreasing trend in crystallinity is observed, the data varies from batch to batch, which causes a large deviation on each data points.

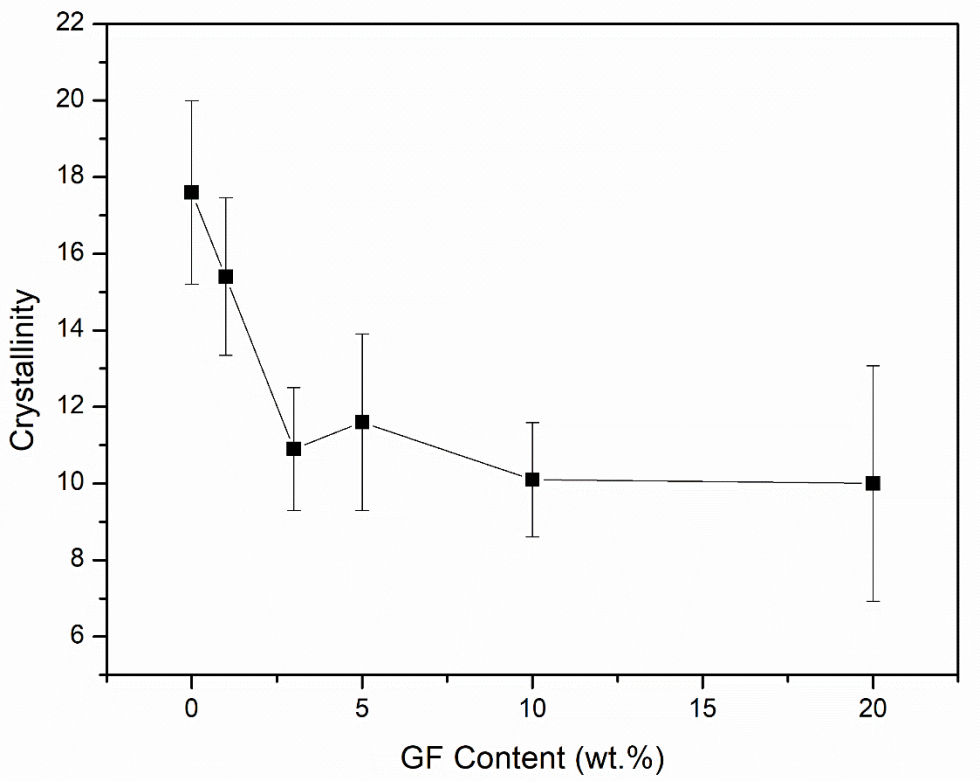

Figure 15 Crystallinity measured by DSC for each composition

The printing conditions also have a large effect on the final performance of the printed parts. Fig. 16 shows a series of 100 % infilled cones 3D printed at a printing speed of 15 mm/s without a cooling fan during printing.

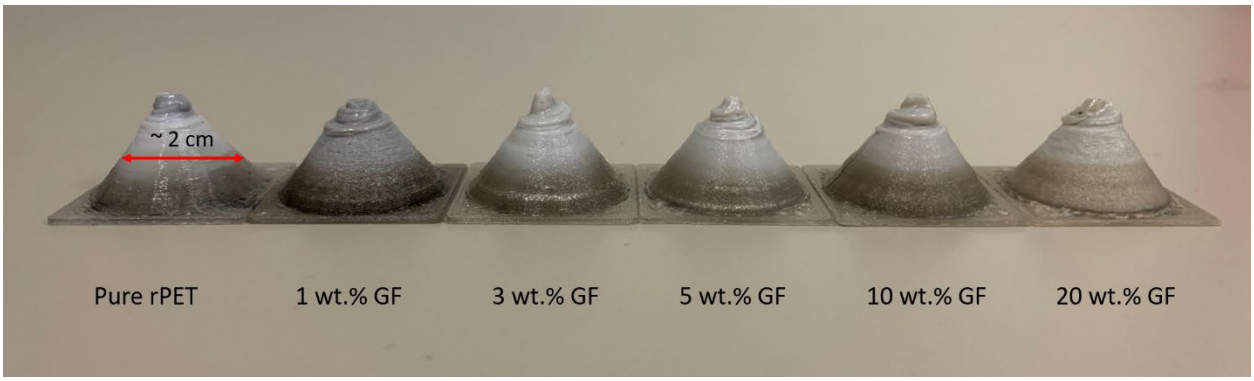

Figure 16 100 % infilled cone geometries printed with rPET/GF filaments

Although GF did decrease the crystallinity of rPET in this study, GF is not considered to be a PET crystallization inhibitor. If there is a continuous heat source to maintain the elevated temperature, rPET/GF composite will still crystallize to the degree that the material shows a brittle fracture under tension load rather than a ductile fracture. Usually for PET, this macroscopic transition in property is indicated by the appearance of white color on the material. This can be observed in the upper portions of the printed cones shown in Fig. 16. This is observed as layering speed increases with shorter layer times associated with the shorter toolpaths at the top of the cones. At these shorter layer times, the previous layer does not have enough time to sufficiently cool down, so it keeps crystallizing during the printing process. To make a more uniform print, it might be necessary to apply a fan cooling and lift the printing nozzle after each layer; however, it is not yet clear how active cooling affects the interlayer bonding. We do not imply that the lower crystallinity form of rPET and its GF composites are better than the higher crystallinity one; however, a printed part with non-uniform properties is not desired. Thus, a topic of further study is how to precisely control the printing process of rPET (or virgin PET) and its composites to enable homogenous material properties throughout the printed shape.

5. CONCLUSIONS AND IMPLICATIONS FOR FUTURE RESEARCH

In this study, the team investigated the influence of GF on the material properties of rPET, its processability for FFF, and the mechanical properties of the resulting printed parts. It was found that GF significantly increased the viscosity of rPET. The size of the GF filler reduces during the multiple extrusion process, which limits its performance in enhancing the ultimate tensile strength of printed parts; however, the increase in modulus with increasing GF was noteworthy, and the results still demonstrate a much better overall mechanical properties than printed ABS and PLA. In addition, the tensile test of printed single layer specimens revealed that increasing the loading of GF will lead to an increase in the anisotropy of printed parts, due to a minor decrease in interlayer bonding strength. Overall, the rPET/GF composite showed both great printability and resultant mechanical properties. Several complex parts were successfully printed, including components for a low-cost drone that was designed for delivery and remote sensing applications in the developing world [36], (Figures 7 and 17).

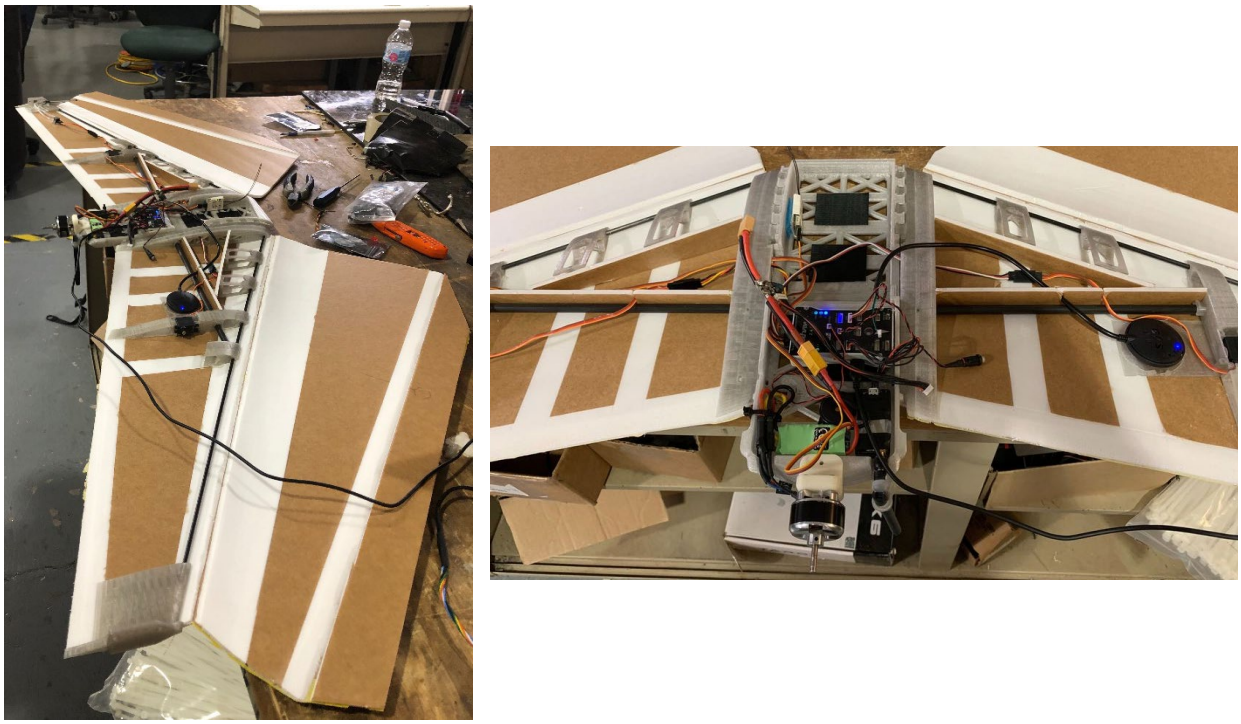

Figure 17 rPET Printed Parts Used in EcoSoar Drone Vehicle

While the material has demonstrated remarkable printability (i.e., absence of warpage and good layer adhesion), it is noted that uneven cooling (due to uncontrolled printing environment and/or to print time between layers) can cause different levels of crystallinity in the final part (e.g., Figure 16). To further refine this approach, and to optimize printed rPET quality for all printed geometries, additional research in FFF heat transfer modeling, rPET crystallization kinetics, and novel FFF toolpath strategies is needed to precisely control the printing process. In addition, the team sees great potential in using rPET as a feedstock for large-scale, deployable FFF printing. By using rPET as a pellet feedstock in a large-scale extruder mounted to a robot arm or gantry system (Figure 18), rPET could be used to fabricate large structural components, tools and dies, fixtures and jigs, and even furniture, for FOBs. To accomplish this goal, additional research would be needed in feedstock preparation (e.g., cleaning and palletization of rPET), process parameter development, and heat transfer and crystallization kinetics modeling for large rPET deposits.

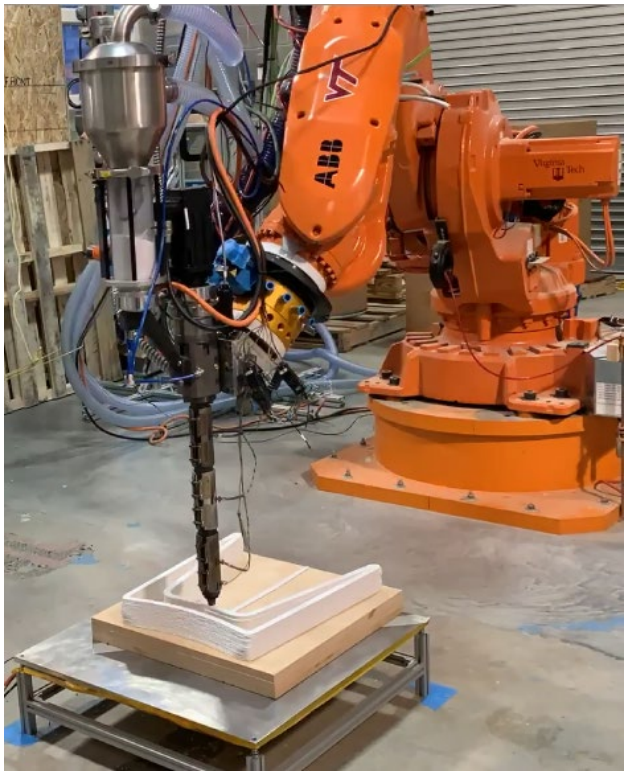

Figure 18 Virginia Tech Large-Scale Robotic Extrusion System, which features a ~8 foot reach and 150 lb/hr pellet extrusion

LITERATURE CITED

[1] M.T. S. Laville, A million bottles a minute: world's plastic binge 'as dangerous as climate change', 2017. https://www.theguardian.com/environment/2017/jun/28/a-million-a-minute-worlds-plastic-bottle-binge-as-dangerous-as-climate-change.
[2] N.A.f.P.C.R. (NAPCOR), Postconsumer PET Container Recycling Activity in 2017, National Association for PET Container Resources (NAPCOR), 2018.
[3] S.D. Cosper, H.G. Anderson, K. Kinnevan, B.J. Kim, Contingency Base Camp Solid Waste Generation, ENGINEER RESEARCH AND DEVELOPMENT CENTER CHAMPAIGN IL CONSTRUCTION …, 2013.
[4] M. Baumers, C. Tuck, R. Wildman, I. Ashcroft, R.J.E. Hague, Energy inputs to additive manufacturing: does capacity utilization matter, 1000(270) (2011) 30-40.
[5] M. Baumers, Economic aspects of additive manufacturing: benefits, costs and energy consumption, © Martin Baumers, 2012.
[6] V. Petrovic, J.V. Haro, O. Jordá, J. Delgado, J.R. Blasco, L. Portolés, Additive Layer Manufacturing: State of the art in industrial applications through case studies, (2010) 1.
[7] N. Mohan, P. Senthil, S. Vinodh, N. Jayanth, A review on composite materials and process parameters optimisation for the fused deposition modelling process, Virtual and Physical Prototyping 12(1) (2017) 47-59.
[8] O.S. Carneiro, A.F. Silva, R. Gomes, Fused deposition modeling with polypropylene, Materials & Design 83 (2015) 768-776.
[9] G. Sodeifian, S. Ghaseminejad, A.A. Yousefi, Preparation of polypropylene/short glass fiber composite as Fused Deposition Modeling (FDM) filament, Results in Physics 12 (2019) 205-222.
[10] S. Chong, G.-T. Pan, M. Khalid, T.C.-K. Yang, S.-T. Hung, C.-M.J.J.o.P. Huang, t. Environment, Physical characterization and pre-assessment of recycled high-density polyethylene as 3D printing material, 25(2) (2017) 136-145.
[11] H. Hamod, Suitability of recycled HDPE for 3D printing filament, (2015).
[12] <PVT testing of polymers under industrial processing conditions.pdf>.
[13] P. Zoller, P. Bolli, Pressure-volume-temperature relationships of solid and molten poly(ethylene terephthalate), Journal of Macromolecular Science, Part B 18(3) (2006) 555-568.
[14] G. Consolati, F. Quasso, An experimental study of the occupied volume in polyethylene terephthalate, The Journal of Chemical Physics 114(6) (2001) 2825-2829.
[15] F. Awaja, D. Pavel, Recycling of PET, European Polymer Journal 41(7) (2005) 1453-1477.
[16] F.J.R. Welle, Conservation, Recycling, Twenty years of PET bottle to bottle recycling—an overview, 55(11) (2011) 865-875.
[17] N.M.L. Mondadori, R.C.R. Nunes, L.B. Canto, A.J. Zattera, Composites of Recycled PET Reinforced with Short Glass Fiber, Journal of Thermoplastic Composite Materials 25(6) (2011) 747-764.
[18] M. Kráčalík, L. Pospíšil, M. Šlouf, J. Mikešová, A. Sikora, J. Šimoník, I. Fortelný, Recycled poly(ethylene terephthalate) reinforced with basalt fibres: Rheology, structure, and utility properties, Polymer Composites 29(4) (2008) 437-442.
[19] M. Kráčalík, L. Pospíšil, M. Šlouf, J. Mikešová, A. Sikora, J. Šimoník, I. Fortelný, Effect of glass fibers on rheology, thermal and mechanical properties of recycled PET, Polymer Composites 29(8) (2008) 915-921.
[20] I. Rezaeian, S.H. Jafari, P. Zahedi, S. Nouri, An investigation on the rheology, morphology, thermal and mechanical properties of recycled poly (ethylene terephthalate) reinforced with modified short glass fibers, Polymer Composites 30(7) (2009) 993-999.
[21] N.E. Zander, M. Gillan, R.H. Lambeth, Recycled polyethylene terephthalate as a new FFF feedstock material, Additive Manufacturing 21 (2018) 174-182.

[22] A. Elamri, A. Lallam, O. Harzallah, L. Bencheikh, Mechanical characterization of melt spun fibers from recycled and virgin PET blends, Journal of Materials Science 42(19) (2007) 8271-8278.
[23] C. Duty, C. Ajinjeru, V. Kishore, B. Compton, N. Hmeidat, X. Chen, P. Liu, A.A. Hassen, J. Lindahl, V. Kunc, What makes a material printable? A viscoelastic model for extrusion-based 3D printing of polymers, Journal of Manufacturing Processes 35 (2018) 526-537.
[24] K. Urman, J.J.J.o.P.S.P.B.P.P. Otaigbe, Novel phosphate glass/polyamide 6 hybrids: miscibility, crystallization kinetics, and mechanical properties, 44(2) (2006) 441-450.
[25] B.J.C. Pukanszky, Influence of interface interaction on the ultimate tensile properties of polymer composites, 21(3) (1990) 255-262.
[26] N.M.L. Mondadori, R.C.R. Nunes, A.J. Zattera, R.V.B. Oliveira, L.B. Canto, Relationship between processing method and microstructural and mechanical properties of poly(ethylene terephthalate)/short glass fiber composites, Journal of Applied Polymer Science 109(5) (2008) 3266-3274.
[27] A. Kelly, a.W.J.J.o.t.M. Tyson, P.o. Solids, Tensile properties of fibre-reinforced metals: copper/tungsten and copper/molybdenum, 13(6) (1965) 329-350.
[28] S.-Y. Fu, B. Lauke, E. Mäder, C.-Y. Yue, X.J.C.P.A.A.S. Hu, Manufacturing, Tensile properties of short-glass-fiber-and short-carbon-fiber-reinforced polypropylene composites, 31(10) (2000) 1117-1125.
[29] Advantex_ECR_glass_properties_ww_201004_web. http://www.ocvreinforcements.com/pdf/library/Advantex_ECR_glass_properties_ww_201004_web.pdf .
[30] R.A. Bubeck, M. Most, T. Zhang, 3D Printing and Evaluation of Novel Nanographene-Containing ABS Thermoplastics, Polymer-Based Additive Manufacturing: Recent Developments, ACS Publications2019, pp. 53-68.
[31] N. Li, Y. Li, S.J.J.o.M.P.T. Liu, Rapid prototyping of continuous carbon fiber reinforced polylactic acid composites by 3D printing, 238 (2016) 218-225.
[32] <Order‐disorder transitions in the extrusion of fiber‐filled poly (ethylene terephthalate) and blends.pdf>.
[33] A.L.F. de M. Giraldi, J.R. Bartoli, J.I. Velasco, L.H.I. Mei, Glass fibre recycled poly(ethylene terephthalate) composites: mechanical and thermal properties, Polymer Testing 24(4) (2005) 507-512.
[34] V.E. Reinsch, L.J.P.c. Rebenfeld, The influence of fibers on the crystallization of poly (ethylene terephthalate) as related to processing of composites, 13(5) (1992) 353-360.
[35] V.E. Reinsch, L.J.J.o.a.p.s. Rebenfeld, Crystallization processes in poly (ethylene terephthalate) as modified by polymer additives and fiber reinforcement, 52(5) (1994) 649-662.
[36] Z.D. Standridge, K.B. Kochersberger, Design, Development, and Range Optimization of Flying Wing UAV, 2018 AIAA/ASCE/AHS/ASC Structures, Structural Dynamics, and Materials Conference, 2018, p. 0567.

General	Include recommendations as to where the glass fibers would be derived from in a FOB setting, for the strengthening of the recycled PET. In addition, a listing of the equipment needed for this operation to be performed on a FOB in a conex such as the granulator, filament extruder, etc. (and the ancillary requirements such as power, gases, water, etc. would greatly benefit the value of this report to DoD (i.e. provide a recipe/menu/manual for accomplishing this on a FOB).
Response Not entered	

Glass fiber will have to be shipped to FOBs for this application, as is mentioned in the List of Equipment Section. Fortunately, these materials are not required in high amounts for the process and are lightweight, so their transport could potentially be low in cost.

Rheology	The results comprising the Newtonian and the shear thinning region were obtained by a sweep. Sweeps are certainly faster to perform, but thixotropic, Non-Newtonian fluids need time to relax to measure true rheological properties. A steady-state experiment should have been performed where the viscosity should be measured for a time at a particular shear rate until equilibrium is reached and then shear rate can be increased. Exp should be run forward and in reverse to measure hysteresis. Although the trends in the power law exponent (Oswald de Waele Power Law model) are likely correct, there are only a few data points from each curve (the shear thinning area only, not including the invalid data point regime with shear stress decreases with increasing shear rate) to determine n. Recommend more data points centered around shear thinning regime using steady state shear flow experiment.
Response Not entered	

A transient stress growth rheology measurement of 20 wt.% GF composites was taken under 1 s^{-1} shear rate, and it can be seen that the time required for the system to reach steady state is less than 1 second,

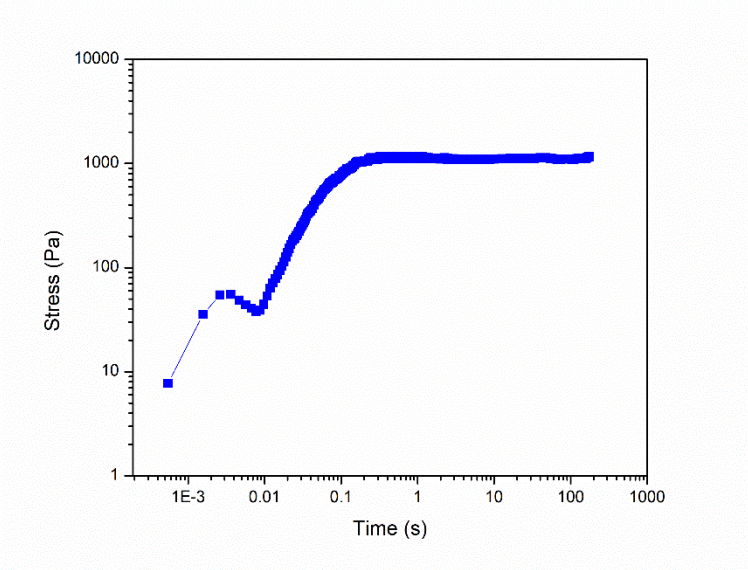

At higher shear rate or lower GF loadings, it will take shorter time to reach steady state, and all the rheology data presented in the manuscript has a wait time of 5 seconds before any data points were taken, so it can be confirmed that data points are taken at equilibrium.

Hysteresis measurement is rarely seen in polymer composite papers, thus we didn't include it in our design of experiments.

	What are the specific metrics for success for this seedling effort? It is not clear
Conclusions and Implications for Future Research	whether those were met because the metrics appear to be only loosely stated - i.e., print PET and show printability with GF. Incorporation of up to 20 wt% GF was successful, but is this enough? The properties are better than pure rPET, but there are various polymers that out perform the rPET/GF composites made in terms of properties. On a larger note, the report does not state what is needed for success for this recycled material to provide significant utility to the Soldier. What properties/performance metrics are required of this program? How much GF will be needed? What print rate and resolution is needed at a minimum to meet soldier needs? How will this work be advanced towards truly enabling the soldier to print improved polymers/composites in the field (i.e., what needs to be done to make a recycling facility to make the feedstock?). on a related note, where will the glass fibers come from? What sources of glass fibers or other reinforcement can be used to improve the properties? Given the measured properties with a modest rise in properties, could particulate filler be used instead of glass fibers to achieve similar properties? There is no comparison in this report to make this judgement.
Response Not entered	

Currently there are no military standards for any 3D printing materials, so instead we compared the properties of printed rPET and its composites with other most popular 3D printing feedstocks (ABS & PLA), in order to demonstrate the feasibility to use this recycled material as fused filament 3D-printing feedstock. The breadth of possible products that could be manufactured in the field using this material is large, as evidenced by our ability to 3D-print drone parts (a rugged and demanding application) from waste PET bottles. Really it will be the goal of the Phase II project to design a robust system that is capable of delivering to soldiers whatever it is they need in a flexible way. A recycling facility in the field would require simple, off-the-shelf, equipment for shredding, label and cap removal, and drying. These are simple operations that can occupy low footprints and use almost no energy.

It could be possible to use other particulate fillers, perhaps some that might be more readily available or supplied to an FOB, to provide an increase in mechanical properties to the 3D-printed PET material. This is something that can be tested during the Phase II portion of this project. The GF will need to be shipped to the FOBs, which is mentioned in the List of Equipment section.

Conclusions and Implications for Future Research	Provide an estimate of energy demands that would be required to operate such a system at an FOB.
Response Not entered	

To shred, clean, and extrude a single bottle into 3D-printable filament, roughly 0.01386 kW • hr is required (1). To 3D print a single bottle's worth of material, roughly 0.0125 kW • hr is required (2, 3). This amounts to 0.02636 kW • hr for a single bottle to go through the entire process.

Therefore, for a system that recycles 39,370 bottles into fully finished 3D printed parts per 8 hours (0.5 metric tons), 129.72 kW will be required to go from dirty bottles to finished, 3D-printed product. This number could be further reduced by using more energy efficient printers as opposed to desktop printers.

1. http://www-g.eng.cam.ac.uk/impee/topics/RecyclePlastics/files/RecyclingEnergyBalance.pdf
2. https://3dstartpoint.com/3d-print-power-consumption-how-much-power-does-a-3d-printer-use/